Enhanced Piezoresponse and Nonlinear Optical Properties of Fluorinated Self-Assembled Peptide Nanotubes

Soma Khanra[a], Sandra V. Vassiliades[b], Wendel A. Alves[b], Kaidi Yang[c], Rainer Glaser[c,d], Kartik Ghosh[e], Payal Bhattacharya[a], Ping Yu[a], and Suchismita Guha[a*]

[a]Department of Physics and Astronomy, University of Missouri, Columbia, MO 65211, USA
[b]Centro de Ciências Naturais e Humanas, Universidade Federal do ABC, 09219-580 Santo André, São Paulo, Brazil
[c]Department of Chemistry, University of Missouri, Columbia, MO 65211, USA
[d]Missouri University of Science and Technology, Rolla, MO 65409, USA
[e]Physics, Astronomy, and Materials Science, Missouri State University, Springfield, MO 65897, USA

Abstract

Self-assembled *L,L*-diphenylalanine (FF) nanostructures offer an attractive platform for photonics and nonlinear optics. The nonlinear optical (NLO) coefficients of FF nanotubes depend on the diameter of the tube [Khanra *et al.* Phys. Chem. Chem. Phys. **19**, 3084 (2016)]. To further enhance the NLO properties of FF, we search for structural modifications. Here, we report on the synthesis of fluorinated FF dipeptide by replacing one ortho-hydrogen atom in each of the phenyl groups of FF by a fluorine atom. Density-functional theoretical calculations yield insights into minimum energy conformers of fluorinated FF (Fl-FF). Fl-FF self-assembles akin to FF into micron-length tubes. The effects of fluorination are evaluated on the piezoelectric response and nonlinear optical properties. The piezoelectric d_{15} coefficient of Fl-FF is found to be more than 10 times higher than that of FF nanotubes, and that the intensity of second

* Corresponding author E-mail; guhas@missouri.edu

harmonic generation (SHG) polarimetry from individual Fl-FF nanotubes is more than 20 times that of individual FF nanotubes. Furthermore, we obtain SHG images to compare the intensities of FF and Fl-FF tubes. This work demonstrates the potential of fluorine substitution in other self-assembled biomimetic peptides for enhancing nonlinear optical response and piezoelectricity.

Nonlinear optical (NLO) phenomena are fundamental to important technological tools in optoelectronics. Proteins are a class of structurally and functionally diverse biopolymers, which are intrinsically chiral, and collagens, muscle tissue, and fibrillar proteins are known to show NLO properties.[1-3] Second harmonic generation (SHG) occurs in materials that do not possess inversion symmetry. In general, a large number of bioinspired materials have non-centrosymmetric crystal structures,[4] and self-assembly of these materials results in hollow tubes which are suitable to measure SHG[5] and optical wave-guiding.[6-8] To improve these materials systematically requires the development of structure-function relationships and attempts to modify the optical properties of the biomaterials without jeopardizing their polar superstructures. *L,L*-diphenylalanine (FF, more correctly named as *L*-phenylalanyl-*L*-phenylalanine) is one prominent dipeptide which has been studied extensively (vide infra). We report here on the design and synthesis of a fluorinated derivative Fl-FF (correctly named as 2-fluoro-*L*-phenylalanyl-2-fluoro-*L*-phenylalanine) which is informed by the analysis of the superstructure of FF. Using similar methods for materials fabrication and characterization,[9] we demonstrate that the properties of the fluorinated material, Fl-FF, greatly exceed those of the parent FF material.

Since the discovery of self-assembly in FF, extensive studies have been carried out to characterize its mechanical rigidity,[10] chemical and thermal stabilities,[11,12] non-reversible phase transition,[12] wave guiding,[13] and chiroptical activity.[14,15] Self-assembled FF micro/nanostructures have been utilized in various applications such as biosensing,[16-18] drug delivery,[19] mechanical reinforcement,[19,20] energy generation,[21,22] organic electronics,[23,24] and photodynamic therapy.[25] The nonlinear optical properties of as-synthesized FF nanotubes are attributed to the material's $P6_1$ non-centrosymmetric space group,[12] which further gives rise to ferroelectricity[26-28] and piezoelectricity.[29]

A key question concerns possibilities for chemical modifications of FF which may allow for an enhancement of the SHG and piezoelectric responses while still maintaining the self-assembly process. Such an approach may substantially advance the area of nanophotonics and open a new realm of self-assembled photonic metamaterials. In this work we take a cue from fluorinated polymers, where the outstanding piezo - and ferroelectric properties of polyvinylidene fluoride (PVDF) have stimulated numerous studies over five decades.[30-32] The introduction of the copolymer poly(vinylidenfluoride-co-trifluoroethylene), P(VDF-TrFE), where one methylene-H atom is replaced by F in the TrFE unit, results in a strong ferroelectric response due to the all *trans*-conformation.[33] The difference in bond dipole moments of the C–H and C–F bonds on opposite sides of the polymer chain leads to a large dipole moment. In these cases the fluorine atom is both part of the NLO chromophore and also directly responsible for the polar alignment of the polymer chains.

Here, self-assembled Fl-FF nanotubes are fabricated using the liquid vapor phase method in analogy to the self-assembly process of FF nanotubes.[9] Detailed SHG polarimetry from FF nanotubes was conducted in Ref.[9], which forms the basis for a comparison of the nonlinear

optical properties of FF and Fl-FF nanotubes. The fluorination of FF in this work involves a function-based design and chemical synthesis. Individual FF and Fl-FF tubes were isolated for SHG polarimetry and piezoelectric force spectroscopy.

The SHG setup is based on a Q-switched YAG:Nd^{3+} laser operating at a wavelength of 1064 nm and was configured either in the transmission geometry with a spot size of 100 μm or in a reflection geometry using a micro-SHG imaging setup. The transmission geometry was discussed in detail Ref. [9]. The SHG imaging in the reflection mode uses a long working distance 20X microscope objective along with a cooled EMCCD camera (Photometrics Evolve 512) for capturing images. The contact mode of the scanning probe microscope (Model: Park-NX10, Park Systems) was used to characterize the surface topography of the samples and the piezo force microscopy (PFM) mode for obtaining the piezo-response images.

The self-assembly of FF has been discussed in several articles.[34, 35] It starts with the packing of six FF dipeptides into a helical macrocycle, where the ammonium and carboxylate groups constitute the inner core of the cycle. An aqueous environment is necessary for the self-organization process, and water remains confined in the interior channel as shown in Fig. 1 (a). The elemental building block of the FF crystal is the FF zwitterion. These FF zwitterions aggregate by intermolecular interactions between positively charged ammonium moieties and negatively charged carboxylate groups and two such ion pairing contacts are highlighted by the orange shading in Fig. 1 (b). This crystal architecture results in chiral helices with six (*S*,*S*)-enantiomers of FF zwitterions per turn, and allows the parallel alignment of the carbonyl groups within the amide functional groups of every one of the FF zwitterions.

Density-functional theory (DFT) calculations[36] employing the SMD solvation model[37] result in several nearly isoenergetic conformations of the benzyl moieties, and two such optimized

structures calculated at the SMD(B3LYP/6-31G*) level are shown in Fig. 1 (c) and (d). The key structural motif is the placement of the Lewis acidic ammonium group and of the Lewis basic carboxylate group in relative proximity but not close enough to form an effective Lewis pair. This "frustrated Lewis pair" motif causes the tight binding of water molecules to bridge the frustrated Lewis pair (Fig. 1 (d)). The bridging water molecule, which acts as a Lewis acid toward the FF's Lewis base and as a Lewis base to the FF's Lewis acid, guides the preparation of materials and serves as the basis for the design of responsive materials. An SEM image of a FF micro/nanotube is shown in Fig. 1 (e).

The NLO response of FF self-assembled tubes likely is the result of the unsymmetrical arene chromophores. In FF itself, the unsymmetrical arenes are of the type peptide–CH_2–C_6H_5, that is, they are mono-alkyl substituted benzenes with the polar axis closely aligned with the C_{ipso}–C_{para} axis (C1–C4). The most obvious way to enhance the intensity of this chromophore would involve the placement of an electron-acceptor in the para-position to afford a standard donor-acceptor disubstituted benzene. However, such a modification would drastically alter the interaction between the helical columns in the FF nanotubes. In contrast, we analyzed the crystal structure of FF in search for the positions of aromatic H atoms that could be replaced by F atoms with the least consequences for the overall crystal architecture. Hence, our focus turned to H/F replacements in the ortho position and the difluorinated FF (Fl-FF) is one of the possible implementations.

Details of Fl-FF synthesis and the synthesis scheme are provided in the Supporting Information. In Fl-FF one ortho-hydrogen atom in each of the phenyl groups of FF is replaced by a fluorine atom. In Fig. 1 (f), the four conformers are shown of water-bridged Fl-FF calculated at the level of SMD(B3LYP/6-31G*) for aqueous solution. The most important result becomes

immediately obvious in that the structure of water-bridged FF (Fig. 1 (d)) is essentially retained in all conformers of water-bridged Fl-FF. In the FF structure (Fig. 1(d)), there are four ortho-positions in the two benzene rings that may be occupied by fluorine in Fl-FF and we label these from left to right as 1 – 4 (see synthesis scheme in Supporting Information). The names of the Fl-FF conformers formally indicate the two ortho-positions that were substituted by fluorine atoms in FF. The most stable structure of Fl-FF is conformer **13** (with fluorine atoms in the 1 and 3 positions of the FF structure), and the relative energies of conformers **23**, **14**, and **24** are shown in kcal/mol. Benzene-benzene T-contacts are observed in all of the conformers. Structures **13** and **14** benefit from hydrogen bonding between the fluorine atom in the 1-position and a proximate ammonium-H.

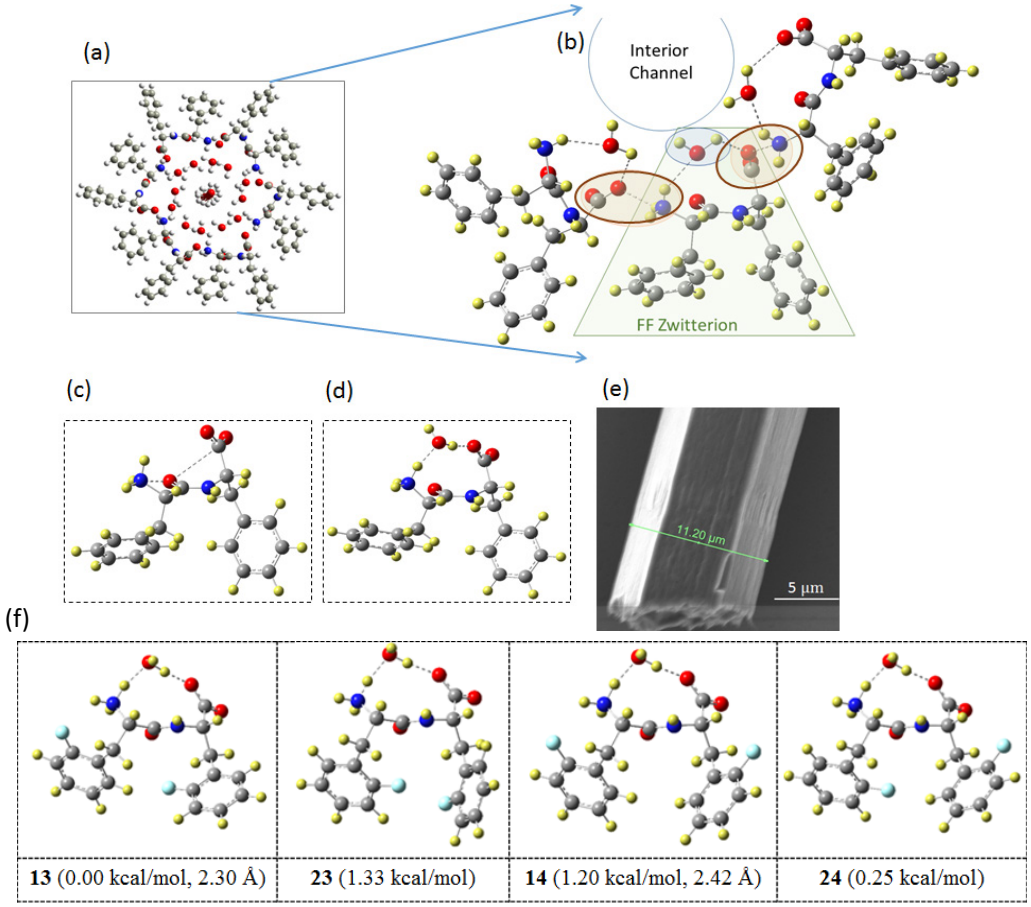

Fig. 1. (a) Chemical structure of a FF macrocycle with water molecules in the core. (b) A segment of the FF macrocycle with one FF zwitterion highlighted by green shading. (c) The SMD(B3LYP/6-31G*) optimized structure of FF zwitterion contains a "frustrated Lewis pair" comprised of a Lewis acid (ammonium group) and a Lewis base (carboxylate) functionality. (d) The SMD(B3LYP/6-31G*) optimized structure of FF zwitterion with a water molecule bridging between the Lewis acid and Lewis base functionalities. (e) SEM image of a self-assembled FF tube. (f) Molecular models of water-bridged Fl-FF zwitterion determined at the SMD(B3LYP/6-31G*) level for aqueous solution. The row below the figures contains the following information: number of the conformer (energy relative to the most stable structure, distance between F atom and proximate ammonium-H atom in Å).

Figure 2 shows the electron microscopy images from Fl-FF. Selected area diffraction from a high resolution transmission electron microscope image shows the crystalline nature of Fl-FF (Fig. 2 (a-b)). Fig. 2 (c-d) show SEM images of a single Fl-FF tube and multiple tubes. The lengths of the tubes may reach a couple of hundred micrometers.

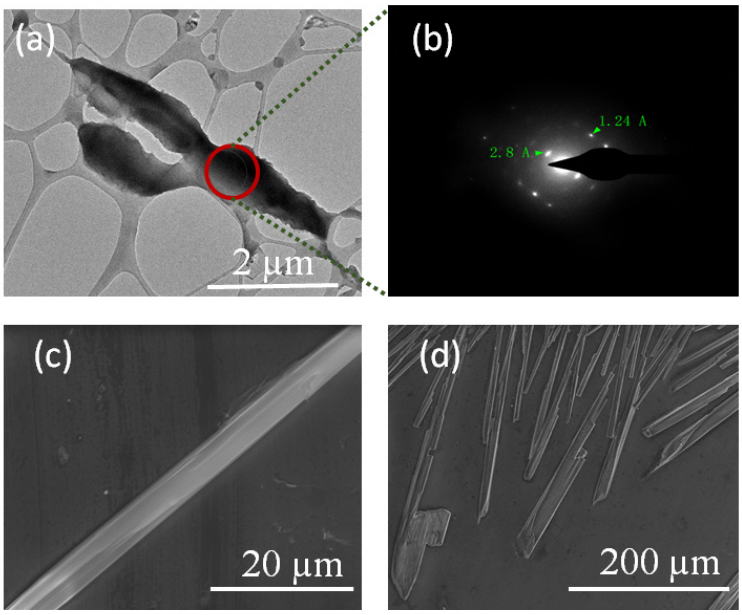

Fig. 2. (a) High-resolution transmission electron microscope image from an Fl-FF nanotube. (b) Selected area electron diffraction from the highlighted area in the image in (a). SEM images of (c) a single Fl-FF nanotube and (d) multiple Fl-FF nanotubes.

To characterize the piezoelectric properties of the FF and Fl-FF samples we collected the PFM images as well as spectroscopy data. Since the nanotubes are on a surface, it is easier to measure the shear deformation by PFM. For optimal comparison of their piezoresponses, FF and Fl-FF nanotubes with similar diameters were chosen. Fig. 3 shows the PFM imaging data of FF and Fl-FF nanotubes. Fig. 3 (a-c) show the topography, phase, and amplitude images of the FF nanotubes, and Fig. 3 (d-f) show the analogous images of the Fl-FF nanotubes. We infer the tube diameters (outer) of both FF and Fl-FF to be approximately 2 μm from the topography images. Large phase as well as amplitude differences in the tube region compared to the non-tube region clearly indicates that both tubes are piezoelectric. To compare the d_{15} value (shear response) of FF and Fl-FF, piezoforce spectroscopic measurements were carried out. Fig. 3 (g) and (h) show the PFM amplitude as a function of the applied dc voltage. In both samples, the amplitude increases with voltage. The measurements were carried out such that the sample response is perpendicular to the cantilever and, hence, our measurements yield the d_{15} component of the piezoelectric tensor. The d_{15} components, deduced from the slopes, are 50 pm/V and 600 pm/V for FF and Fl-FF nanotubes, respectively.

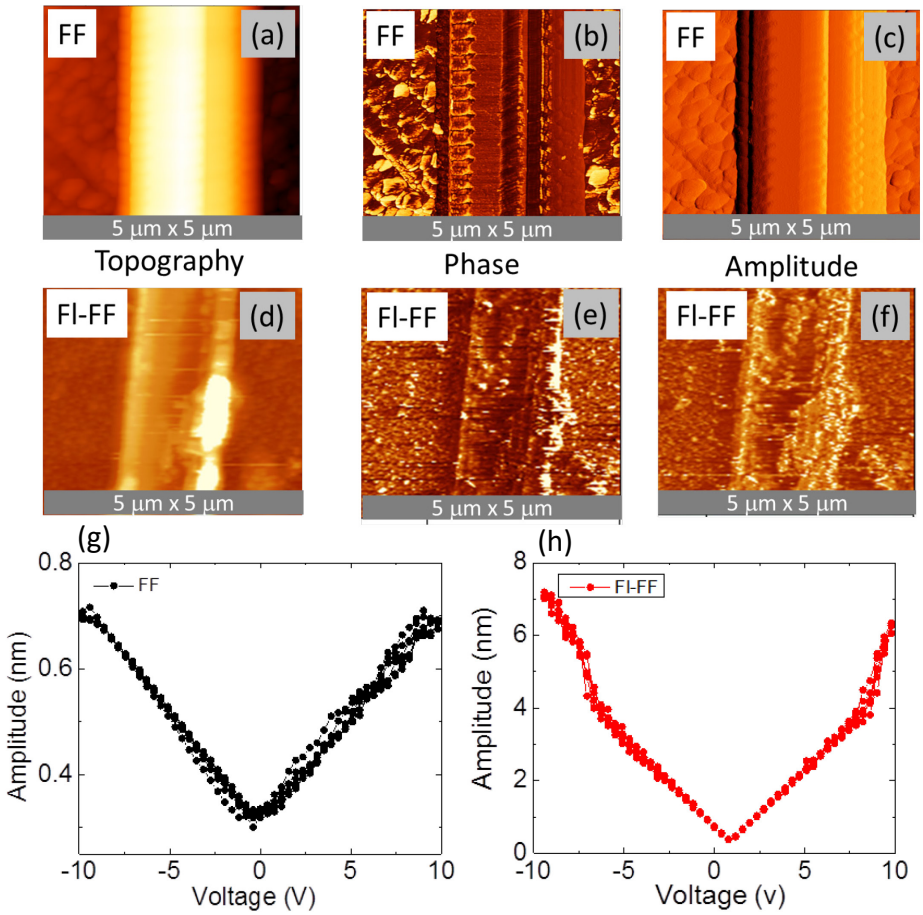

Fig. 3. Piezoresponse force microscopy images of FF (top row) and Fl-FF (bottom row). (a)-(c) Topography, phase, and amplitude images of the FF nanotube. (d)-(f) Topography, phase, and amplitude images of the Fl-FF nanotube. (g) Local amplitude piezoresponse loop from FF nanotube. (h) Localized amplitude piezoresponse loop from Fl-FF nanotube.

Figure 4 (a) shows the tube orientation during SHG measurements in the transmission geometry, where the fundamental electric field was incident normal to the sample, and its polarization at an angle Ψ relative to the laboratory axis was rotated by a half wave plate from 0° to 180°. The SHG parallel (*p* polarization) and perpendicular (*s* polarization) polarizations with respect to the tube axis were measured using a linear polarizer. For selecting individual Fl-FF and FF tubes, a long working distance microscope with a CCD camera was used.

Figure 4 (c-d) show the SEM images of Fl-FF and FF nanotubes, respectively, where the parameters of the tube size may be used for SHG comparison. The SHG intensity is known to increase with the tube diameter, as was observed in FF nanotubes.[9] Fig. 4 (b) plots the SHG intensity for two varying FF nanotubes with diameters 8 μm (circle) and 13 μm (square). To compare the SHG intensity of Fl-FF with FF, we consider a Fl-FF tube with a diameter approximately 3.5 times lower compared to the diameter of the FF tube.

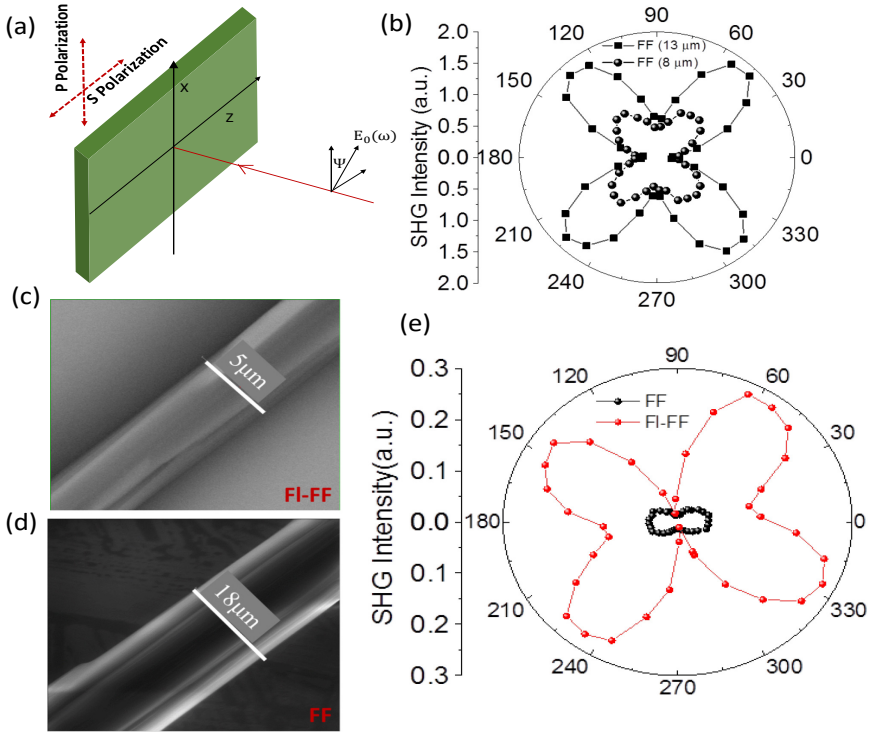

Fig. 4. (a) Orientation of the sample in the transmission SHG experiment. (b) Total SHG intensity from FF nanotubes with two different outer diameter nanotubes. The black square symbols correspond to a 13 μm FF nanotube and the black circular symbols correspond to an 8 μm FF nanotube. (c) SEM image of the Fl-FF nanotube and (d) SEM image of the FF nanotube used in the SHG experiment. (e) Total SHG intensity from FF (black circle) and Fl-FF (red circle) nanotube.

Fig. 4 (e) compares the SHG intensity (*s* polarization) between FF and Fl-FF. The SHG intensity of the Fl-FF (for a 5 μm tube) is six times higher than the SHG intensity of the FF (for

an 18 μm tube). Scaling the SHG intensity to account for the difference in the tube diameter yields a factor of 20 by which the intensity of Fl-FF is higher compared with FF. If we compare the *p* polarization (Figure S3) data from Fl-FF with Fl-FF, we observe a different SHG polarimetry pattern. The *p* polarization data from Fl-FF nanotube has only two peaks as compared to the four peaks from FF nanotubes. This suggests that either Fl-FF has a different symmetry compared to the $P6_1$ symmetry of FF nanotubes or has different nonlinear optical coefficients compared to FF. Determining the exact symmetry of Fl-FF nanotubes is the subject of our future work. We discuss a few possible symmetry considerations based on the SHG signature of Fl-FF in the Supporting Information.

We have also obtained SHG images from FF and Fl-FF tubes using a microscope objective and a cooled CCD camera. Figs. 5 (a) and (b) compare the bright-field image and the SHG image for the same tubes of the Fl-FF sample. The SHG image was captured in 5 s; it clearly shows the edge of the tubes. In order to compare the SHG images from FF and Fl-FF, we chose tubes of similar diameters. The bright-field and SHG images are superimposed in Figs. 5 (c) and (d). The blue rectangle depicts the tube that was illuminated and the yellow square shows the SHG intensity. The SHG image for Fl-FF in Fig. 5 (c) was obtained in 5 s compared to the SHG image of FF in Fig. 5 (d), which is very weak and was obtained in 60 s. These SHG images are again a direct proof that Fl-FF has a higher SHG efficiency compared to only FF.

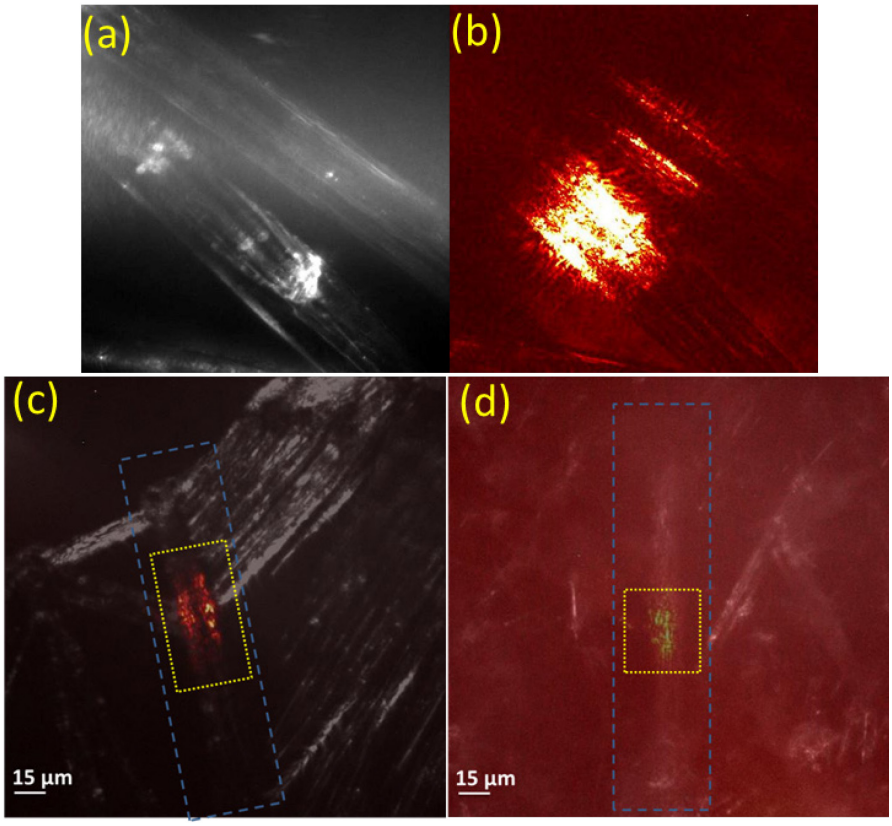

Fig. 5. (a) Bright-field image of Fl-FF tubes. (b) SHG image from the same Fl-FF tubes shown in (a). To compare the SHG intensity from FF and Fl-FF tubes, we selected tubes of similar diameters. (c) and (d) show the SHG image superimposed on the bright-field image of Fl-FF and FF tubes. The blue rectangle depicts the tube that was illuminated and the yellow rectangle shows the SHG intensity. For the same laser power and geometry, the SHG images were obtained in 5 s for Fl-FF (c) and in 60 s for FF in (d).

In summary, fluorination of di-peptides that self-assemble into micro/nanostructures may have a significant impact in the area of nonlinear optics and piezoelectricity. Fluorinated FF dipeptide, Fl-FF, which was synthesized by replacing H with F in the ortho position self-assembles into tubular structures, similar to FF micro/nanotubes, opening up a path for probing nonlinear optical and piezoresponse properties. The piezoresponse coefficient (d_{15}) of a Fl-FF tube of outer diameter close to 2 µm was found to be 600 pm/V. A similar diameter tube of FF

yields a piezoresponse of only 50 pm/V. Similarly, SHG polarimetry from Fl-FF tubes show at least 20 times higher intensity compared to FF nanotubes. Direct SHG images from FF and Fl-FF tubes further provide evidence of a higher SHG efficiency for the fluorinated sample compared to only FF. DFT calculations were performed to find the minimum energy conformations of Fl-FF. This work not only demonstrates the potential of fluorinated self-assembled biological nanostructures in enhancing nonlinear optical and piezoresponse properties, it also provides a critical test for the future development of improved first principles approaches for guiding synthesis of such peptide molecules.

SUPPLEMENTARY MATERIAL

See Supplementary materials for Synthesis, NMR spectra, and fitting of the SHG polarimetry data.

ACKNOWLEDGEMENTS

This research was supported in part by the US National Science Foundation ECCS-1707588 (SG) and CHE-1665487 (RG). RG acknowledges the donors of the American Chemical Society Petroleum Research Fund (PRF-53415-ND4) for partial support of this research. WAA acknowledges the São Paulo Research Foundation (FAPESP grant no. 2017/02317-2).

References

1. S. Roth and I. Freund, J. Chem. Phys. **70** (4), 1637-1643 (1979).
2. R. M. Williams, W. R. Zipfel and W. W. Webb, Biophysical Journal **88** (2), 1377-1386 (2005).
3. F. Tiaho, G. Recher and D. Rouède, Opt. Express **15** (19), 12286-12295 (2007).
4. C. H. Görbitz, Chem. Eur. J. **13** (4), 1022-1031 (2007).
5. A. Handelman, S. Lavrov, A. Kudryavtsev, A. Khatchatouriants, Y. Rosenberg, E. Mishina and G. Rosenman, Adv. Opt. Mater. **1** (11), 875-884 (2013).
6. Q. Li, H. Ma, A. Wang, Y. Jia, L. Dai and J. Li, Adv. Opt. Mater. **3** (2), 194-198 (2015).
7. Q. Li, Y. Jia, L. Dai, Y. Yang and J. Li, ACS Nano **9** (3), 2689-2695 (2015).
8. X. Yan, J. Li and H. Möhwald, Adv. Mater. **23** (25), 2796-2801 (2011).
9. S. Khanra, K. Ghosh, F. F. Ferreira, W. A. Alves, F. Punzo, P. Yu and S. Guha, Phys. Chem. Chem. Phys. **19** (4), 3084-3093 (2017).
10. N. Kol, L. Adler-Abramovich, D. Barlam, R. Z. Shneck, E. Gazit and I. Rousso, Nano Lett. **5** (7), 1343-1346 (2005).
11. J. Ryu and C. B. Park, Biotechnol. Bioeng. **105** (2), 221-230 (2010).
12. A. Heredia, I. Bdikin, S. Kopyl, E. Mishina, S. Semin, A. Sigov, K. German, V. Bystrov, J. Gracio and A. L. Kholkin, J. Phys. D: Appl. Phys. **43** (46), 462001 (2010).
13. A. Handelman, B. Apter, N. Turko and G. Rosenman, Acta Biomaterialia **30**, 72-77 (2016).
14. J. George and K. G. Thomas, J. Am. Chem. Soc. **132** (8), 2502-2503 (2010).
15. J. M. Slocik, A. O. Govorov and R. R. Naik, Nano Lett. **11** (2), 701-705 (2011).
16. S. Kogikoski, C. P. Sousa, M. S. Liberato, T. Andrade-Filho, T. Prieto, F. F. Ferreira, A. R. Rocha, S. Guha and W. A. Alves, Phys. Chem. Chem. Phys. **18** (4), 3223-3233 (2016).
17. C. P. Sousa, M. D. Coutinho-Neto, M. S. Liberato, L. T. Kubota and W. A. Alves, J. Phys. Chem. C **119** (2), 1038-1046 (2015).
18. B.-W. Park, R. Zheng, K.-A. Ko, B. D. Cameron, D.-Y. Yoon and D.-S. Kim, Biosens. Bioelectron. **38** (1), 295-301 (2012).
19. M. S. Liberato, S. Kogikoski, E. R. da Silva, D. R. de Araujo, S. Guha and W. A. Alves, Journal of Materials Chemistry B **4** (8), 1405-1413 (2016).
20. N. Even, L. Adler-Abramovich, L. Buzhansky, H. Dodiuk and E. Gazit, Small **7** (8), 1007-1011 (2011).
21. V. Nguyen, R. Zhu, K. Jenkins and R. Yang, Nat. Commun. **7**, 13566 (2016).
22. A. Levin, T. C. T. Michaels, L. Adler-Abramovich, T. O. Mason, T. Muller, B. Zhang, L. Mahadevan, E. Gazit and T. P. J. Knowles, Nature Phys. **12** (10), 926-930 (2016).
23. S. Khanra, M. Abdullah-Al Mamun, F. F. Ferreira, K. Ghosh and S. Guha, ACS Applied Nano Materials **1** (3), 1175-1187 (2018).
24. S. Khanra, T. Cipriano, T. Lam, T. A. White, E. E. Fileti, W. A. Alves and S. Guha, Adv. Mater. Interf. **2**, 1500265-1500274 (2015).
25. M. I. Souza, Y. M. Jaques, G. P. de Andrade, A. O. Ribeiro, E. R. da Silva, E. E. Fileti, É. d. S. Ávilla, M. V. B. Pinheiro, K. Krambrock and W. A. Alves, J. Phys. Chem. B **117** (9), 2605-2614 (2013).
26. I. Bdikin, V. Bystrov, S. Kopyl, R. P. G. Lopes, I. Delgadillo, J. Gracio, E. Mishina, A. Sigov and A. L. Kholkin, Appl. Phys. Lett. **100** (4), 043702 (2012).

27. V. S. Bystrov, E. Seyedhosseini, S. Kopyl, I. K. Bdikin and A. L. Kholkin, J. Appl. Phys. **116** (6), 066803 (2014).
28. A. Handelman, P. Beker, N. Amdursky and G. Rosenman, Phys. Chem. Chem. Phys. **14** (18), 6391-6408 (2012).
29. A. Kholkin, N. Amdursky, I. Bdikin, E. Gazit and G. Rosenman, ACS Nano **4** (2), 610-614 (2010).
30. H. Kawai, Jpn. J. Appl. Phys. **8** (7), 975 (1969).
31. R. G. Kepler and R. A. Anderson, J. Appl. Phys. **49** (3), 1232-1235 (1978).
32. A. J. Lovinger, Science **220** (4602), 1115-1121 (1983).
33. Q. M. Zhang, V. Bharti and X. Zhao, Science **280** (5372), 2101-2104 (1998).
34. C. H. Gorbitz, Chem. Commun. (22), 2332-2334 (2006).
35. R. F. Silva, D. R. Araújo, E. R. Silva, R. A. Ando and W. A. Alves, Langmuir **29** (32), 10205-10212 (2013).
36. C. J. Cramer, *Essential of Computational Chemistry*. (John Wiley and Sons, 2004).
37. A. V. Marenich, C. J. Cramer and D. G. Truhlar, J. Phys. Chem. B **113** (18), 6378-6396 (2009).